The Electronically Excited States of LH2 Complexes from *Rhodopseudomonas acidophila* Strain 10050 Studied by Time-Resolved Spectroscopy and Dynamic Monte Carlo Simulations. II. Homo-Arrays Of LH2 Complexes Reconstituted Into Phospholipid Model Membranes

Tobias J. Pflock,[†] Silke Oellerich,[†] Lisa Krapf,[†,‡] June Southall,[§] Richard J. Cogdell,[§] G. Matthias Ullmann,[⊥] and Jürgen Köhler[†,*]

[†] Experimental Physics IV and BIMF, University of Bayreuth, D-95440 Bayreuth, Germany

[§] Institute of Molecular, Cell and Systems Biology, College of Medical Veterinary and Life Sciences, Biomedical Research Building, University of Glasgow, Glasgow G12 8QQ, Scotland, U.K.

[⊥] Computational Biochemistry/Bioinformatics, University of Bayreuth, D-95440 Bayreuth, Germany

S *Supporting Information*

ABSTRACT: We performed time-resolved spectroscopy on homoarrays of LH2 complexes from the photosynthetic purple bacterium *Rhodopseudomonas acidophila*. Variations of the fluorescence transients were monitored as a function of the excitation fluence and the repetition rate of the excitation. These parameters are directly related to the excitation density within the array and to the number of LH2 complexes that still carry a triplet state prior to the next excitation. Comparison of the experimental observations with results from dynamic Monte Carlo simulations for a model cluster of LH2 complexes yields qualitative agreement without the need for any free parameter and reveals the mutual relationship between energy transfer and annihilation processes.
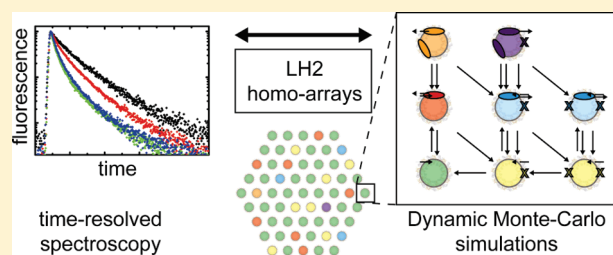
INTRODUCTION

In photosynthesis, a specialized pigment—protein complex, the photochemical reaction center (RC), acts as the key transducer.[1] It contains a dimer of (bacterio)chlorophyll ((B)Chl) molecules, called the special pair, which is the primary electron donor for the electron transfer chain. On the basis of the absorption cross section of a Chl molecule and the number of photons provided from the sun, an order of magnitude estimate yields that under optimum conditions the special pair would absorb about one photon per second.[1,2] This number is in contrast to the turnover rate of the RC which is in the kHz range.[3,4] From this rough calculation, it becomes clear that the exploitation of sunlight as a source for energy requires an efficient light-harvesting apparatus for collecting as many photons as possible. In photosynthesis, this is accomplished by a network of antennas, i.e., pigment—protein complexes that capture photons and transfer the excitation energy with high efficiency to the RC.[5-8] Thereby, the number of Chl molecules organized in antennas and serving a light harvesting function usually exceeds a few hundred per RC.[9-13]

For purple photosynthetic bacteria, these antenna complexes consist of pairs of polypeptides ($\alpha\beta$) that noncovalently bind a small number of bacteriochlorophyll (BChl) and carotenoid (Car) molecules. These modules then oligomerize to produce

the native circular or elliptical complexes, called LH1 and LH2,[14-19] which are described in more detail in part I.[54]

An obvious question that arises concerns the performance of a network of antenna complexes as a function of the illumination conditions and which has attracted many groups to investigate this issue.[20-24] On the basis of phenomenological approaches that included singlet—singlet annihilation,[25,26] these studies allowed the development a coarse-grained picture of the supramolecular organization of the photosynthetic unit and estimates to be obtained for the transition rates between the electronic states before the high resolution structural data became available. However, a systematic study of the energy transfer properties of natural membrane patches (chromatophores) has been hampered due to the unknown stoichiometric ratio of LH2/RC-LH1 complexes.[8,11,27]

In the preceding paper (part I),[54] we have detailed the rich photophysics of isolated, noninteracting, LH2 complexes on the picosecond time scale. By combining time-resolved spectroscopy and generalized dynamic Monte Carlo (DMC) simulations, we

were able to explain the experimental observations quantitatively without the need for any free parameters. Here we extend this study to the question of energy migration within homoarrays of LH2 complexes reconstituted into phospholipid model membranes, which is a first step toward a quantitative understanding of the initial processes of energy migration in photosynthesis. The spatial arrangement of the pigment—protein complexes has been verified by atomic force microscopy and cryo-transmission electron microscopy. The energy transfer reactions within such arrays have been investigated by time-resolved spectroscopy on the ps time scale, as a function of both the photon fluence incident onto the sample and the repetition rate of the excitation pulses. The first parameter determines the density of excitations within the array, while for a given fluence, the latter parameter is related to the number of LH2 complexes that carry a triplet state prior to the next excitation pulse. The experimental results are compared with results from DMC simulations, and it is found that the performance of such arrays is largely determined by a complex interplay of singlet—singlet annihilation and singlet—triplet annihilation processes.

■ MATERIALS AND METHODS

Materials. As phospholipids, we used 1,2-dioleoyl-sn-glycerol-3-phosphocholine (DOPC) and 1,2-dioleoyl-sn-glycerol-3-phosphoglycerol (DOPG) (Avanti Polar Lipids, Alabaster, USA). The detergent Octyl-β-D-glucopyranoside (β-OG) was obtained from Fluka (St. Gallen, Switzerland) and Glycyl-Glycin (GlyGly) buffer from Roth (Karlsruhe, Germany).

The LH2 complexes from the species *Rhodopseudomonas acidophila* (strain 10050) were purified as described previously.[28,29] Subsequently, they were dissolved in 50 mM Glygly (Glycyl-Glycin, Roth, Karlsruhe, Germany) at pH 8 and 1% β-OG (Octyl-β-D-glucopyranoside, Fluka, St. Gallen, Switzerland).

Membrane Reconstitution. In order to create an appropriate lipid environment for the LH2 complexes, these were reconstituted into prefabricated liposomes with a defined lipid composition. This is done via a detergent mediated reconstitution, as has been described previously.[30,31] Briefly, we prepared lipid films from a DOPC/DOPG mixture (4/1, weight ratio, w/w). For the vesicle preparation, we resuspended the lipid films in 50 mM Glygly buffer (pH 8) at a concentration of 2 mg/mL and vortexed them to achieve complete hydration of the films. Then we prepared unilamellar vesicles by sequential extrusion of the lipid suspension through polycarbonate membranes (Avanti Polar Lipids, USA) with decreasing pore size diameter of 0.8, 0.2, 0.1, and 0.05 μm respectively (Avanti protocol). After preparation, the vesicles were used immediately for membrane reconstitution. For the detergent mediated reconstitution, the appropriate amount of detergent-solubilized LH2 sample was added to the prefabricated DOPC/DOPG liposomes in order to yield an average lipid—protein ratio of 500/1 and 2500/1 (concentration ratio, c/c), respectively. Assuming a molar mass of 1.3×10^5 g/mol for the LH2 complexes and approximately 0.8×10^3 g/mol for a lipid molecule, the c/c ratios of 500/1 and 2500/1 correspond to w/w ratios of 3/1 and 15/1, respectively. The LH2-liposome suspension was then put into a Slide-A-Lyzer dialysis cassette and dialyzed against a reservoir of detergent-free buffer at 6 °C in a dark environment for 3 days. After that, the reconstituted LH2 complexes were stored at 4 °C in the dark and used within, at most, 3 days.

The unilamellarity and homogeneity of the LH2-containing liposomes was investigated by cryo-transmission electron
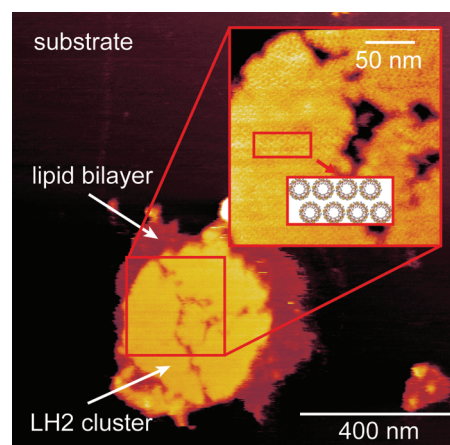

Figure 1. Raw data of an AFM image from LH2-containing DOPC/DOPG proteoliposomes adsorbed on a mica substrate (lipid—protein ratio 500/1, c/c). The boxed region is shown at higher resolution in the inset (top right), revealing the hexagonal ordering of the LH2 complexes, as indicated schematically. The AFM data have been processed using Gwyddion (Czech Metrology Institute), the schematic representation of the LH2 complexes has been created using Rasmol.

microscopy (see Supporting Information). From that we obtained a size distribution of the liposomes of diameters between 50 - 80 nm. The quality of the reconstitution after dialysis was checked by absorption spectroscopy. From the constant B800/B850 peak absorption ratio of 0.8 and the lack of an absorption band from free BChl *a*, both before and after reconstitution, we verified the structural integrity of the LH2 complexes.

Atomic Force Microscopy. For the AFM measurements, we diluted 2 μL of the LH2-containing lipid vesicles in 100 μL of AFM buffer (20 mM Glygly, pH 8, 150 mM NaCl) and brought this onto a freshly cleaved mica substrate. In order to increase adsorption on the substrate, we added 50 mM $CaCl_2$. The sample was then adsorbed for about 5 min and thoroughly rinsed afterward with excess buffer in order to wash away unadsorbed proteoliposomes. In the next step, the sample was covered with H_2O and placed below the cantilever unit of the AFM imaging head (PicoSPM, Molecular Imaging). Images were taken with a noninvasive oscillating cantilever mode (MAC mode, Molecular Imaging) with varying spatial resolution, depending on the size of the image detail. The raw data have been processed and analyzed with the computer programmes Gwyddion (free AFM software, Czech Metrology Institute) and ImageJ (free imaging software National Institutes of Health, USA).

Time-Resolved Fluorescence Spectroscopy. For the time-resolved experiments, the same setup that has been described already in part I[54] has been used. Before and after each measurement, the integrity of the LH2 samples was checked by absorption spectroscopy, from which significant bleaching or irreversible sample damage could be excluded.

■ RESULTS

Atomic Force Microscopy. In order to visualize the microscopic arrangement of the LH2 complexes within the proteoliposomes, we employed atomic force microscopy (AFM). Figure 1 shows the raw data of an AFM image from a cluster of LH2 complexes reconstituted into a DOPC/DOPG double layer that is adsorbed on a mica surface. The structure corresponds to three proteoliposomes that probably have merged during the adsorption

process. The image allows to distinguish three different height levels: The mica substrate displayed in dark brown color, the DOPC/DOPG bilayer displayed in dark red, and the clusters of LH2 complexes displayed in yellow. The cluster of LH2 complexes in the boxed region is shown at higher resolution in the inset of the figure which clearly uncovers a pattern of hexagonally arranged LH2 rings with a center-to-center distance of 7–8 nm. A dimerization of the complexes or a significant tilt of the complexes with respect to the mica surface as reported previously[32,33] is not observable.

Time-Resolved Fluorescence Decays. The emission spectra of the reconstituted LH2 complexes show a small red shift of about 1 nm with respect to the samples in detergent, which is in agreement with previous work.[34] The energy transfer properties of the LH2 complexes embedded in model membranes were studied by time-resolved spectroscopy as a function of the excitation fluence, J_{EX} (number of photons/(pulse·cm^2)) and the repetition rate k_{REP}. Since the spectral profile of the time-resolved emission spectra did not depend on the excitation parameters, the transient signal was integrated over the entire emission band. For a fluence of 26×10^{12} photons/(pulse·cm^2) and a repetition rate of 81 MHz, the fluorescence decays are compared in Figure 2 for two reconstituted samples (c/c lipid
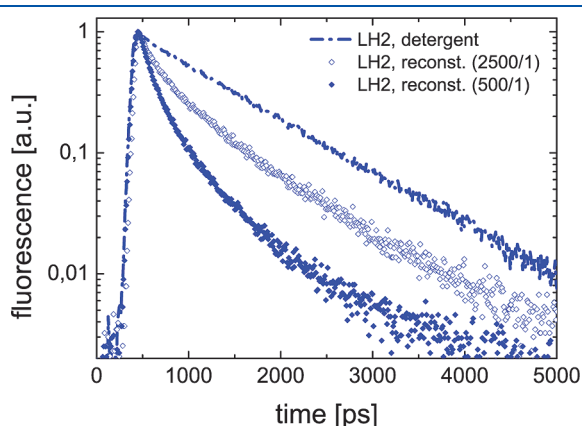
protein ratios 2500/1 open diamonds; 500/1 filled diamonds) and the detergent-solubilized sample (dash-dotted line, see also part I[54]). While the detergent-solubilized LH2 complexes feature a monoexponential decay, the fluorescent transients of the membrane-reconstituted complexes are clearly not monoexponential and decay the faster the lower the lipid—protein ratio, i.e., the higher the average LH2 concentration per lipid vesicle.

This quenching effect was further investigated as a function of both the excitation fluence and the repetition rate, Figure 3. Interestingly, all fluorescence decays observed are also clearly not monoexponential. For a lipid—protein ratio of 500/1 and a repetition rate of 2 MHz, Figure 3A shows the variation of the fluorescence decay as a function of the fluence. The observation is that an increase of the fluence leads to stronger quenching of the fluorescence. Similarly, Figure 3B shows for the same sample and a fluence of 26×10^{12} photons/(pulse·cm^2) the transients as a function of the repetition rate. An increase of the repetition rate from 50 kHz over 2 to 8 MHz leads to a faster decay of the fluorescence. Yet a further increase of the repetition rate from 8 to 81 MHz has no additional effect on the fluorescence transients.

A relative measure that allows the comparison of the various transients is the emission yield, i.e., the time-integrated relative emission intensity. For the different repetition rates, these integrals are shown in Figure 4 as a function of the fluence for the two lipid—protein ratios. At a repetition rate of 50 kHz, some data points are missing due to the low signal. For all repetition rates, the data reveal a decrease of the emission yield for an increase of the fluence. At the lipid—protein ratio of 500/1, Figure 4A, one finds for a fixed fluence a systematic decrease of the emission yield upon increasing the repetition rate from 50 kHz to 8 MHz and within experimental accuracy no further decrease of the emission yield for an increase of the repetition rate to 81 MHz. Only at a fluence of 3.3×10^{12} photons/(pulse·cm^2) is the emission yield at 8 MHz significantly higher than that at 81 MHz. At the lipid—protein ratio of 2500/1, Figure 4B, the emission yields are generally higher than for the low lipid—protein ratio, see also Figure 2. For all repetition rates, we find a decrease of the yield for increasing fluence and for a fixed fluence a decrease of the yield for an increase of the repetition rate.

(Monte Carlo) Simulations. *The Model.* In order to describe the fluorescence decays of the membrane reconstituted LH2 complexes, we use as a starting point the model that has been introduced in part I.[54] Briefly, an individual LH2 complex is approximated as a three-level system, see Figure 4A in part I,[54]

Figure 2. Normalized fluorescence decays of LH2 complexes for an excitation fluence of 26×10^{12} photons/(pulse·cm^2) and a repetition rate of 81 MHz for isolated LH2 complexes in detergent (dash-dotted line), see also paper I, and membrane-reconstituted LH2 complexes for a c/c lipid—protein ratio of 2500/1 (open diamonds) and 500/1 (filled diamonds).
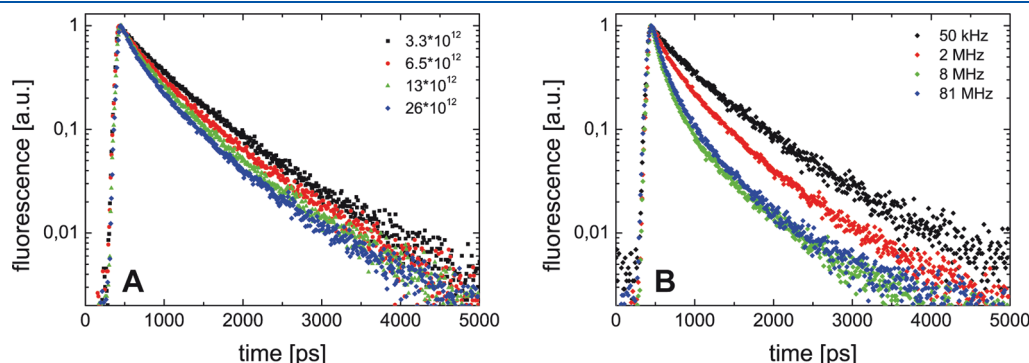

Figure 3. Normalized fluorescence decays of membrane-reconstituted LH2 complexes for a c/c lipid—protein ratio of 500/1 as a function of the excitation parameters. (A) Repetition rate 2 MHz. Fluences in photons/(pulse·cm^2): 3.3×10^{12} (black squares), 6.5×10^{12} (red circles), 13×10^{12} (green triangles), and 26×10^{12} (blue diamonds). (B) Fluence 26×10^{12} photons/(pulse·cm^2). Repetition rates: 50 kHz (black squares), 2 MHz (red circles), 8 MHz (green triangles), and 81 MHz (blue diamonds).
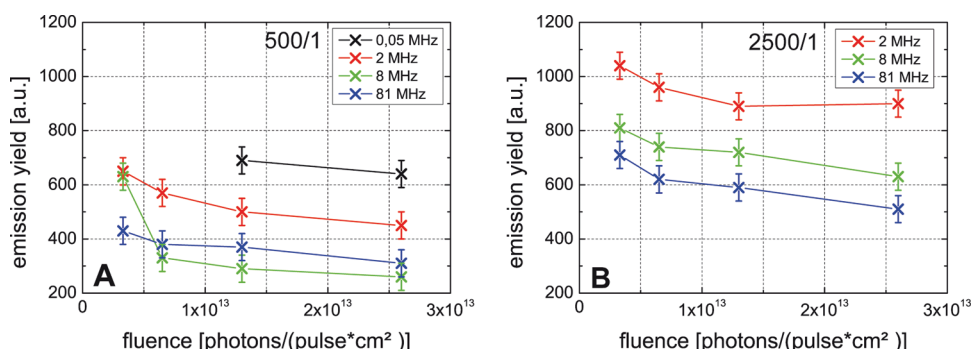
Figure 4. Emission yields of the normalized fluorescence decays of membrane-reconstituted LH2 complexes as a function of excitation fluence and repetition rate. The applied repetition rates were 50 kHz (black, only in part A), 2 MHz (red), 8 MHz (green) and 81 MHz (blue), respectively. The lines connecting the data points serve as a guide for the eye, the error bars correspond to ± 50 au: (A) c/c lipid−protein ratio 500/1; (B) c/c lipid−protein ratio 2500/1.
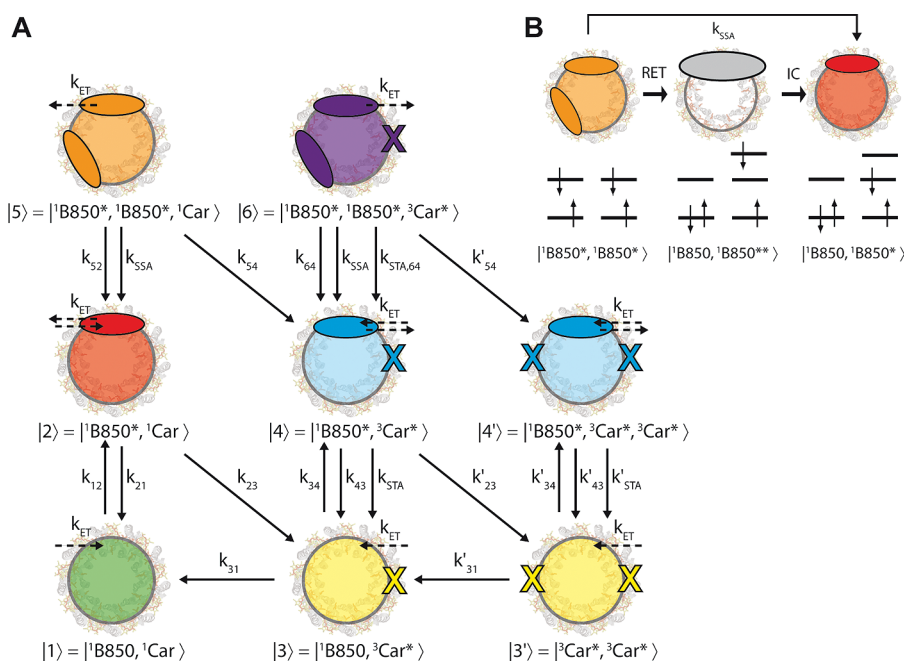

Figure 5. (A) Schematic representation of the model describing the transitions between electronic states of LH2 complexes reconstituted into a membrane environment. The model is an expansion of the model for noninteracting LH2 complexes given in Figure 4C, part I,[54] extended for intercomplex energy transfer between adjacent complexes with a rate k_{ET} (dashed) and singlet−singlet annihilation with a rate k_{SSA}. The nomenclature of the states and the transition rates is explained in the text. (B) Simplified scheme for the singlet−singlet annihilation process adapted from ref 35. The upper part indicates the transition of a LH2 complex with two independent singlet excitations (orange) to a LH2 complex with a higher excited singlet state (gray) that decays to the lowest excited singlet state (red), and symbolizes intracomplex resonance energy transfer (RET) and subsequent internal conversion (IC). The bottom part corresponds to a description in terms of one-electron molecular orbitals. For more details, see text.

with an electronic ground state $|1\rangle = |^1B850, {}^1Car\rangle$, Figure 5A, green, an electronically excited singlet state $|2\rangle = |^1B850*, {}^1Car\rangle$, Figure 5A, red, and an excited triplet state $|3\rangle = |^1B850, {}^3Car*\rangle$, Figure 5A, yellow, located on one of the carotenoid molecules. Excitation of a LH2 complex that already carries a triplet state results in the formation of state $|4\rangle = |^1B850*, {}^3Car*\rangle$, Figure 5A, blue. Possible transitions between these states are governed by rates k_{ij} ($i,j = 1, ..., 4$) and the additional rate $k_{q,43} = k'_{23} + k_{STA}$. The latter rate takes into account that the singlet excitation of state $|4\rangle$ can decay either by intersystem crossing with a rate k'_{23} to the triplet state of another carotenoid molecule on the LH2 ring to a state abbreviated as $|3'\rangle = |^3Car*, {}^3Car*\rangle$, or via singlet−triplet annihilation with a rate k_{STA} back to state $|3\rangle$. As described in detail

in part I,[54] this model quantitatively explains, without free parameters, all experimental observations on isolated, noninteracting LH2 complexes.

For the membrane reconstituted LH2 complexes, we have to consider, in addition, that the singlet excitations located on a LH2 complex can diffuse spatially within the cluster of LH2 complexes. This is taken into account by a rate k_{ET} that describes the transfer of a singlet excitation between adjacent LH2 complexes. The process is incorporated in the schematics of Figure 5A by the dashed arrows. We note that these arrows refer to transitions between states located on adjacent LH2 complexes, while all other arrows refer to transitions between states located on the same LH2 complex. In contrast to the noninteracting
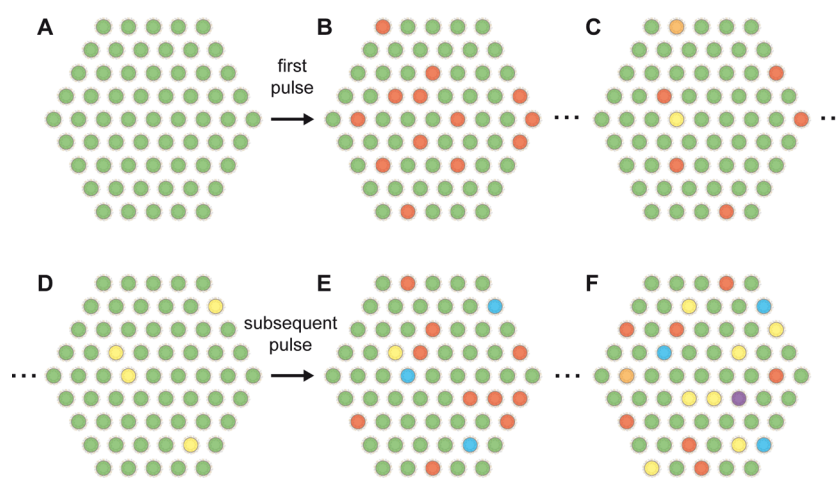
Figure 6. Schematic description of the temporal evolution of the electronic excitations in a model cluster consisting of 61 LH2 complexes arranged in a regular hexagonal pattern. Each circle denotes one LH2 complex, the color of which encodes the states $|1\rangle - |6\rangle$. The sequence from **A** to **F** corresponds to progressing time.

complexes studied in part I,[54] where we excluded doubly singlet-excited LH2 complexes due to the low excitation intensities, here we have to consider now that a singlet-excited LH2 (red), receives another singlet excitation by energy transfer resulting in the state $|5\rangle = |^1B850^*, {}^1B850^*, {}^1Car\rangle$, Figure 5A, orange. Similarly this can happen with a LH2 ring in state $|4\rangle = |^1B850^*, {}^3Car^*\rangle$, which corresponds to a LH2 complex that carries already a singlet and a triplet excitation and leads to the creation of state $|6\rangle = |^1B850^*, {}^1B850^*, {}^3Car^*\rangle$, Figure 5A, purple, with two independent B850 singlet excitations. The two singlets on the same LH2 complex in states $|5\rangle$ and $|6\rangle$ give rise to singlet—singlet annihilation that can be understood analogously to the singlet—triplet annihilation process detailed in part I.[54] In terms of one-electron molecular orbitals, state $|5\rangle$ corresponds to a configuration as displayed at the bottom of Figure 5B. By (intraring) resonance energy transfer (RET) one of the electrons in the upper orbital can be promoted to a higher lying orbital while the other electron is moved simultaneously to the lower orbital, Figure 5B center. This electronic configuration corresponds to a higher excited singlet state ($^1B850^{**}$) on the LH2 indicated by the big gray ellipse. By internal conversion (IC), this state can relax nonradiatively to state $|2\rangle$, Figure 5B, right.[35] Since the time scale of both RET and IC are beyond the resolution of our experiment, we describe the total process by one effective singlet—singlet annihilation rate k_{SSA}. Moreover, since k_{SSA} is about one order of magnitude larger with respect to k_{ET}, we exclude the option that states $|5\rangle$ or $|6\rangle$ receive another singlet excitation via energy transfer and neglect triply singlet-excited LH2 complexes. We take into account radiative decay of state $|5\rangle$ to state $|2\rangle$ with a rate k_{52} which we set equal to $2 \cdot k_{21}$, because at room temperature both excited singlets in state $|5\rangle$ can decay independently. Moreover both $^1B850^*$ excitations can undergo intersystem crossing to the triplet manifold[36] with a rate k'_{54} which we set to $2 \cdot k_{23}$. Singlet—singlet annihilation of state $|6\rangle$ is treated analogously as for state $|5\rangle$. The respective fluorescence decay rate of state $|6\rangle$, k_{64}, is also set to $2 \cdot k_{21}$. In addition, state $|6\rangle$ can decay by intersystem crossing of one of the singlet states or by singlet—triplet annihilation. The first decay channel results in the formation of a LH2 complex with one singlet excitation ($^1B850^*$) and two triplet excitations ($^3Car^*$) on different carotenoids, which we denote as $|4'\rangle = |^1B850^*, {}^3Car^*, {}^3Car^*\rangle$, whereas the latter decay channel corresponds to a transition from state $|6\rangle$ to state $|4\rangle$. The total decay rate for these two processes is $k_{q,64} = k'_{54} + k_{STA,64}$. Analogously to

the transition from $|5\rangle$ to $|4\rangle$ we set $k'_{54} = 2 \cdot k_{23}$, and approximate $k_{STA,64} \approx 2 \cdot k_{STA}$, which yields $k_{q,64} \approx 2 \cdot k_{q,43} = 2 \cdot (k_{23} + k_{STA})$. The model used for the DMC simulations is summarized in Figure 5 and does not consider the migration of triplet excitations (inter- and intracomplex triplet energy transfer), which is justified for the same reasons as detailed in part I.[54] With respect to the model for the noninteracting LH2 complexes (see part I[54]), only two new parameters are introduced: The energy transfer rate k_{ET} and the singlet—singlet annihilation rate k_{SSA}.

An example of a sequence of possible processes within a cluster of LH2 complexes is visualized schematically in Figure 6, which shows a hexagonal pattern of 61 circles, each representing one LH2 complex. Initially, all LH2 complexes are in the electronic ground state $|1\rangle$ (green dots), Figure 6A. By the first laser pulse, some of them are excited to the singlet state $|2\rangle$ (red dots), Figure 6B. These singlet excitations can decay radiatively (fluorescence), cross over to the triplet state $|3\rangle$ (yellow dot), or migrate within the cluster and occasionally meet another singlet excitation resulting in a higher excited singlet state $|5\rangle$ (orange dot), Figure 6C. As the system evolves, the only states that are left prior to the next excitation pulse are the triplet states $|3\rangle$ (yellow dots), Figure 6D. Then, there is a finite probability that a subsequent excitation pulse creates not only new singlet states $|2\rangle$ (red dots) but also leads to a few LH2 complexes that carry both a singlet and a triplet state, $|4\rangle$ (blue dots), Figure 6E. As the system evolves further in time, subsequent laser pulses lead to the population of all the states considered in the model, Figure 6F, see also the movie in the Supporting Information. By reference to Figure 6, we can develop a qualitative understanding of the influence of the excitation parameters on the fluorescence transients. Increasing the fluence creates more "red" states within the array of LH2 complexes. Since these states are mobile, this increases the probability that two "red" states meet, giving rise to singlet—singlet annihilation and thereby enhancing the fluorescence quenching. Increasing the repetition rate corresponds to a higher occupation of "yellow" states prior to the next excitation pulse. Because of the mobility of the "red" states, this increases the probability for the creation of "blue" states and concomitantly for singlet—triplet annihilation, also resulting in an enhanced quenching of the fluorescence. These qualitative considerations show already that in clusters of LH2 complexes, an intricate

Table 1. Pairs of States of Adjacent LH2 Complexes That Qualify for Intercomplex Energy Transfer[a]

$\lvert 2\rangle, \lvert 1\rangle \rightarrow \lvert 1\rangle, \lvert 2\rangle$	$\lvert 4\rangle, \lvert 1\rangle \rightarrow \lvert 3\rangle, \lvert 2\rangle$	$\lvert 5\rangle, \lvert 1\rangle \rightarrow \lvert 2\rangle, \lvert 2\rangle$	$\lvert 6\rangle, \lvert 1\rangle \rightarrow \lvert 4\rangle, \lvert 2\rangle$
$\lvert 2\rangle, \lvert 2\rangle \rightarrow \lvert 1\rangle, \lvert 5\rangle$	$\lvert 4\rangle, \lvert 2\rangle \rightarrow \lvert 3\rangle, \lvert 5\rangle$	$\lvert 5\rangle, \lvert 2\rangle \rightarrow \lvert 2\rangle, \lvert 5\rangle$	$\lvert 6\rangle, \lvert 2\rangle \rightarrow \lvert 4\rangle, \lvert 5\rangle$
$\lvert 2\rangle, \lvert 3\rangle \rightarrow \lvert 1\rangle, \lvert 4\rangle$	$\lvert 4\rangle, \lvert 3\rangle \rightarrow \lvert 3\rangle, \lvert 4\rangle$	$\lvert 5\rangle, \lvert 3\rangle \rightarrow \lvert 2\rangle, \lvert 4\rangle$	$\lvert 6\rangle, \lvert 3\rangle \rightarrow \lvert 4\rangle, \lvert 4\rangle$
$\lvert 2\rangle, \lvert 4\rangle \rightarrow \lvert 1\rangle, \lvert 6\rangle$	$\lvert 4\rangle, \lvert 4\rangle \rightarrow \lvert 3\rangle, \lvert 6\rangle$	$\lvert 5\rangle, \lvert 4\rangle \rightarrow \lvert 2\rangle, \lvert 6\rangle$	$\lvert 6\rangle, \lvert 4\rangle \rightarrow \lvert 4\rangle, \lvert 6\rangle$

[a] The two states to the left of the arrow correspond to the initial states on adjacent LH2 complexes (before energy transfer), for example $\lvert 2\rangle, \lvert 1\rangle$, and the states to the right of the arrow correspond to the final states on adjacent LH2 complexes (after energy transfer), for example $\lvert 1\rangle, \lvert 2\rangle$.

interplay of energy transfer, singlet—singlet annihilation, and singlet—triplet annihilation leads to a stronger fluorescence quenching as compared with the case of noninteracting LH2 complexes.

The DMC Algorithm. In order to determine a "typical" size of a cluster of reconstituted LH2 complexes, we estimate the number of LH2 complexes, N_{LH2}, in a cluster from $4\pi R_{vesicle}^2 = N_{LH2}A_{LH2} + N_{lipid} 0.5 A_{lipid}$, where $R_{vesicle} = 25{-}40$ nm is the size of the vesicles (taken from cryo TEM data, cf. Supporting Information), $A_{LH2} = 50$ nm^2 is the area covered by one LH2 complex, N_{lipid} is the number of lipids and $A_{lipid} = 0.5$ nm^2 is the area covered by the headgroup of one lipid molecule. The factor $^1/_2$ arises from the fact that we have to consider a lipid bilayer for the lipid vesicle formation. For a lipid—protein ratio of 500/1 (2500/1) this yields $N_{LH2} \approx 45{-}115$ (12—30). Therefore, we have chosen for the DMC simulations a cluster size of 61 LH2 complexes, arranged in a hexagonal pattern, see also Figure 1. Each of the 61 model complexes can reside in one of the states $\lvert 1\rangle$ to $\lvert 6\rangle$. Thus, for the whole array we arrive at $6^{61} \approx 10^{47}$ coupled rate equations, demonstrating once more that even for the substantial simplifications made for the description of the multichromophoric LH2 complexes, an analytical treatment of the problem is out of reach.[37] For the DMC simulations we apply the algorithm as detailed in part I[54] with some modifications.[38] First, following the same formalism as detailed previously, it is set for each individual complex in the cluster whether it is excited by a laser pulse. Next we compute the sum K of all possible transition rates including intercomplex energy transfer. For an individual complex in the cluster, the sum of the rates of the intracomplex transitions is given analogously as in part I[54] as $K_{i_l}^{(1)} = \sum_{j=1}^J K_{i_l,j}^{(1)}$. Here i_l denotes state $\lvert i\rangle$ ($i = 1,...6$) of complex l ($l = 1, ..., N$), where N is the number of complexes in the simulated cluster, and the sum runs over all possible J transitions that are connected to state i_l. In order to determine the sum of all transition rates of the entire cluster the $K_{i_l}^{(1)}$ are summed over all complexes and additionally energy transfer processes between pairs of LH2 complexes are taken into account. This yields

$$K = \sum_{l=1}^{61} K_{i_l}^{(l)} + \sum_{ET\ pairs} k_{ET} \qquad (1)$$

The first part of the summation corresponds to the sum of all *intra*complex transitions whereas the second part of the summation corresponds to *inter*complex transitions (energy transfer). The latter process is allowed only for adjacent LH2 complexes and only if these complexes reside in states that are suited to participate in singlet excitation energy transfer. A list of all pairs of states (on adjacent LH2 complexes) that qualify for this process is given in Table 1. In order to compute eq 1 correctly with respect to the energy transfer processes, the mutual arrangement of the LH2 complexes within the array is important. In total this parametrization leads to 6^{61} possible states of the cluster each featuring one specific realization for the value of K. Similarly as before two random numbers, ρ_1 and ρ_2, are chosen from a

uniform distribution between 0 and 1. According to $\Delta t = (1/K) \ln(1/(\rho_1))$, the first random number determines the time interval *when* the next quantum jump occurs. The second random number ρ_2, determines *which* change of the status of the cluster occurs by comparing $(\sum_{\lambda=1}^\mu k_\lambda)/K \le \rho_2 < (\sum_{\lambda=\mu+1}^L k_\lambda)/K$. Here the k_λ represent the individual transition rates that contribute to the specific K of the current status of the cluster. From the comparison, the process corresponding to the index μ is selected to occur next. Then the status of the cluster is updated, the next DMC cycle is initiated, and the whole sequence is repeated until the time $1/k_{Rep}$ has elapsed. The whole process starts over again with the next excitation cycle of the cluster. For one simulation, 10^5 excitation cycles are computed and all transitions that correspond to the emission of a fluorescence photon, i.e., k_{21}, k_{43}, k_{52}, and k_{64}, are counted and fed into a histogram providing the respective fluorescence decay.

In order to apply this algorithm to our model cluster, we have to specify only the two newly introduced parameters, i.e. the singlet—singlet annihilation rate k_{SSA} and the energy transfer rate k_{ET}. From the results of refs 39 and 40, we set the singlet—singlet annihilation rate to $k_{SSA} = (1\ ps)^{-1}$. According to ref 40, at room temperature the $^1B850^*$ singlet state is delocalized over 2—4 BChl a molecules and therefore unable to "sense" the electronic configuration of an adjacent LH2 complex. This simplification has been used successfully to model singlet—singlet annihilation in LDAO-LH2 aggregates[41] and justifies that we consider only one energy transfer rate whatever pairs of states are involved in this process, i.e. we use the same energy transfer rate for processes $\lvert 2\rangle, \lvert 1\rangle \rightarrow \lvert 1\rangle, \lvert 2\rangle$; $\lvert 2\rangle, \lvert 2\rangle \rightarrow \lvert 1\rangle, \lvert 5\rangle$; etc. As a numerical value we use $k_{ET} = (10\ ps)^{-1}$ that has been obtained theoretically from a generalized Förster approach for *Rb. sphaeroides*.[42] This value agrees with the results from a very recent theoretical study where the influence of bath fluctuations on the transfer rate was investigated. These authors found energy transfer times between 8 and 11 ps depending on their model parameters.[43] Experimental data obtained on chromatophores, although not equivalent to the homo arrays of LH2 complexes employed here, pointed also to energy transfer times in the range of some picoseconds.[44] Since all other rate constants have been specified already in part I,[54] we arrive at a full set of input parameters for the DMC simulations as summarized in Table 2.

Results of the DMC Simulations. An example for the simulated fluorescence decays as a function of the fluence is shown in Figure 7 for a repetition rate of 81 MHz. The simulated results reproduce qualitatively the observed decrease of the fluorescence yield for increasing fluence. Yet, in contrast to the experimental findings, all simulated transients are compatible with a biexponential decay with a fast component (τ_{fast}) decaying within some ten ps, and a slow component (τ_{slow}) decaying within about 1 ns. In Table 3, the decay times are summarized together with the associated amplitudes (A_{fast}, A_{slow}). While both decay times, τ_{fast} and τ_{slow} as well as A_{slow} decrease for increasing fluence, A_{fast} changes in the opposite direction. The simulated fluorescence decays as a function of the repetition rate are shown in Figure 8A

8826

dx.doi.org/10.1021/jp2023583 |*J. Phys. Chem. B* 2011, 115, 8821–8831

Table 2. Input Values of the Transition Rates Used for the DMC Simulation of the Membrane-Reconstituted LH2 Complexes

| transfer rates	values $[s^{-1}]$	ref
$k_{12} \rightarrow p_{12}$	$J_{EX}\sigma_{800}$	
k_{21}	8.8×10^8	this work (cf. part I[54])
$k_{23}\ (=k'_{23})$	5×10^7	52
k_{31}	1.4×10^5	53
$k_{34} \rightarrow p_{34}$	$= p_{12} = J_{EX}\sigma_{800}$	
k_{43}	$= k_{21} = 8.8 \times 10^8$	
$k_{q,43} = k'_{23} + k_{STA}$	1.8×10^8	this work (cf. part I[54])
k_{52}, k_{64}	$= 2 \cdot k_{43} = 17.6 \times 10^8$	
k_{54}	$= 2 \cdot k_{23} = 1 \times 10^8$	
$k_{q,64} = k'_{54} + k_{STA,64}$	$= 2 \cdot k_{q,43} = 3.6 \times 10^8$	
k_{ET}	1×10^{10}	42
k_{SSA}	1×10^{12}	40
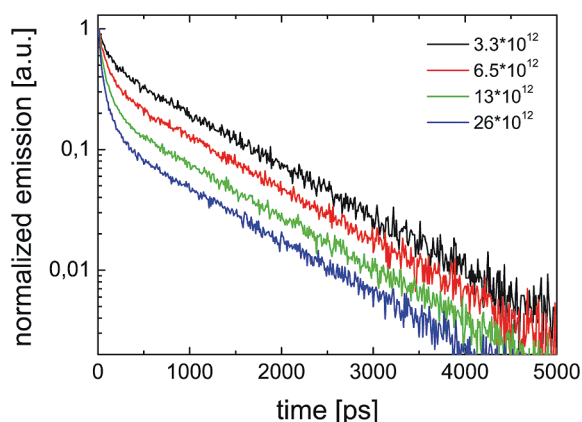
Figure 7. Simulated fluorescence decays for a repetition rate of 81 MHz as a function of the excitation fluence, given in photons/(pulse·cm²): 3.3×10^{12} (black), 6.5×10^{12} (red), 13×10^{12} (green), and 26×10^{12} (blue).

Table 3. Decay Times and Associated Amplitudes of the Simulated Biexponential Fluorescence Decays as a Function of the Fluence for a Repetition Rate of 81 MHz As Shown in Figure 6

fluence [photons/ (pulse·cm²)]	A_{fast}	τ_{fast} [ps]	A_{slow}	τ_{slow} [ps]	ratio A_{fast}/A_{slow}
3.3×10^{12}	0.49	90	0.53	1000	0.92
6.5×10^{12}	0.67	80	0.35	1000	1.9
13×10^{12}	0.76	70	0.21	980	3.6
26×10^{12}	0.82	60	0.14	960	5.9

for the example of a fluence of 26×10^{12} photons/(pulse·cm²). At all repetition rates, the simulated transients feature a fast and a slow decay component. Except for some slight differences in the slow components, the decay curves are not significantly different, which is in clear contrast to the experimental observations. There we found a stronger quenching of the fluorescence for higher repetition rates, see Figure 3B.

As discussed already in paper I,[54] the only state with a lifetime in the order or longer than the inverse of the repetition rate is state $|3\rangle$, corresponding to a LH2 complex with one of the Car
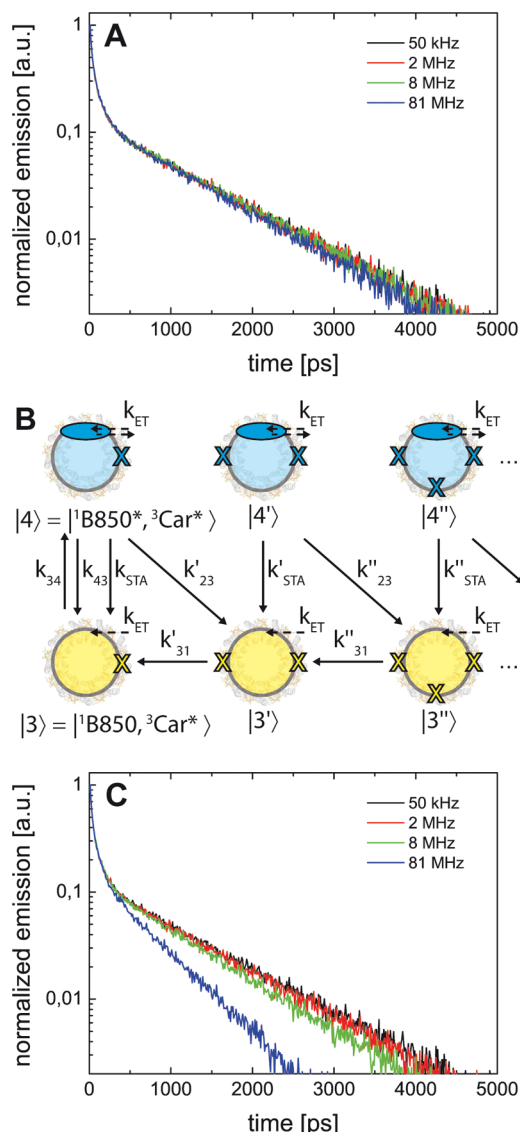
Figure 8. (A) Simulated fluorescence decays for a fluence of 26×10^{12} photons/(pulse·cm²) as a function of the repetition rate: 50 kHz (black), 2 MHz (red), 8 MHz (green), and 81 MHz (blue). (B) Schematic representation of the creation of multiple triplet states on one LH2 complex between two excitation pulses due to intercomplex (singlet) energy transfer. (C) Simulated fluorescence decays for a fluence of 26×10^{12} photons/(pulse·cm²) and for increasing the numerical value of the rate $k_{q,43}$ to 2×10^9 s^{-1} as a function of the repetition rate: 50 kHz (black), 2 MHz (red), 8 MHz (green), and 81 MHz (blue).

molecules residing in the triplet state. For the DMC simulations we neglected LH2 complexes with multiple triplet excitations as indicated by the states $|3'\rangle$, $|3''\rangle$, etc., Figure 8B. The assumption was that this is justified by the encouraging results of paper I,[54] where we found quantitative agreement between experiment and simulations without taking such states into account. However within the cluster, excitation energy transfer between adjacent LH2 complexes is in competition with other decay processes for the $^1B850^*$ states, and because in our calculations $k_{ET} \gg k_{23}$, k_{STA}, the built up of a dominant triplet population, as it was observed in paper I, is suppressed. This explains why we find only a minor influence of the repetition rate on the simulated fluorescence transients.

However, in the cluster, the transitions between states $|3\rangle$ and $|4\rangle$ also need a more sophisticated treatment. In contrast to the isolated, noninteracting LH 2s, which can cross over from $|3\rangle$ to $|4\rangle$ only by another optical excitation, the LH2 complexes within the cluster can also undergo this transition by receiving an excitation from an adjacent LH2 complex by energy transfer. This increases the probability for transitions from $|3\rangle$ to $|4\rangle$ in the clusters tremendously and as a consequence, the relative number of LH2 complexes with multiple triplet excitations on different Car molecule also increases, see Figure 8B. With respect to the noninteracting LH2 complexes, this results in an enhancement of both triplet–triplet annihilation and singlet–triplet annihilation. While triplet–triplet annihilation reduces the number of triplet excitations on one LH2 complex, singlet–triplet annihilation reduces the number of singlet excitations, which is equivalent to the reduction of fluorescing states. Hence, with respect to the average triplet population, these two processes work in opposite directions. Yet here, triplet–triplet annihilation is less important: (I) Because of the short-range exchange interaction, this process will only be effective if the same Car molecule on the same LH2 complex receives two triplet excitations, and (II) triplet–triplet annihilation decreases the number of triplet states on one LH2 ring but the total number of LH2 complexes carrying at least one triplet state, i.e., the count of the number of states $|3\rangle$, $|3'\rangle$, $|3''\rangle$ etc., is not affected. As pointed out already in paper I,[54] the singlet–triplet annihilation rate is determined by resonance energy transfer (RET) and subsequent internal conversion (IC). In particular the rate for RET depends crucially on the details of the electronic configuration of the excited states such as the extent of the electron densities in the triplet and singlet states. As a consequence of this, it can be expected that the rate for singlet–triplet annihilation will be larger the more triplet states are located on an individual LH2 complex. Therefore, we ascribe the discrepancy between the experimental results, Figure 3B, and the simulations, Figure 8A, to an underestimation of the singlet–triplet annihilation process due to having neglected LH2 complexes with multiple triplet excitations. In contrast to the situation of noninteracting LH2 complexes, where it was sufficient to describe this process with a single rate k_{STA}, here it is necessary to also take into account higher-order singlet–triplet annihilation rates, k'_{STA}, k''_{STA}, see Figure 8B.

We wanted to test the hypothesis that an altered singlet–triplet annihilation rate gives rise to a more pronounced dependence of the fluorescence transients on the repetition rate in the clusters. Since a quantitative treatment of the higher-order singlet–triplet annihilation rates is far beyond the scope of the present paper, and because we want to avoid the introduction of a couple of additional parameters, k'_{STA}, k''_{STA}, we followed a pragmatic approach and repeated the DMC simulations with a rate $k_{q,43} = k'_{23} + k_{STA} = 2 \times 10^9 \, s^{-1}$ that was increased by 1 order of magnitude with respect to the former simulations. The results are shown in Figure 8C. Again the transients feature a fast and a slow decay component, but now the trend that a higher repetition rate yields a stronger quenching of the fluorescence can be reproduced qualitatively.

■ DISCUSSION

First we want to address the origin of the biexponential fluorescence decays in the simulated curves, Figures 7 and 8, in more detail and then discuss possible reasons for the quantitative discrepancies between the experimental and simulated fluorescence

transients. For the $^1B850^*$ excitations, energy transfer (time constant 10 ps) outcompetes radiative decay (time constant 1000 ps) by orders of magnitude. Hence, energy transfer and, if two $^1B850^*$ excitations meet on the same complex, subsequent singlet–singlet annihilation (time constant 1 ps) is by far the most efficient quenching mechanism for the $^1B850^*$ excitations within the array of LH2 complexes. This is manifested in the fast decay component. The slow component of the simulated transients simply reflects the decay (either radiatively or via singlet–triplet annihilation) of the "last" $^1B850^*$ state that has survived in the cluster.

Since singlet–singlet annihilation is much faster than energy transfer, the fast time constant corresponds directly to the time that elapses until two singlet excitations arrive at the same LH2 complex. This interpretation is consistent with an increase of this time constant from 60 to 90 ps upon decreasing the excitation fluence, i.e. lowering the density of $^1B850^*$ states in the cluster. This interpretation is consistent as well with the experimental observation that the fluorescence quenching is stronger for a lower lipid-to-protein ratio, see Figure 2. The lower this ratio, the more LH2 complexes (and the more $^1B850^*$ excitations) are present in the cluster increasing the probability for singlet–singlet annihilation and thereby reducing the number of states that can contribute to the fluorescence signal. These findings suggest that for our excitation conditions, a $^1B850^*$ excitation can migrate over 5–10 LH2 complexes. It is instructive to estimate the number of energy transfer steps for a situation with exactly one $^1B850^*$ excitation on the entire cluster. From the ratio of the fluorescence lifetime and the energy transfer time it follows that a $^1B850^*$ excitation can visit about 100 LH2 complexes. Assuming a random walk for the energy migration, this indicates that one $^1B850^*$ excitation that it is not exposed to annihilation processes can sample at most an area with a radius of about 10 LH2 complexes.

While the DMC simulations reproduce qualitatively the experimental observations, there remains a discrepancy in their quantitative agreement. At first glance, this is a bit disappointing, given the positive experiences with the simulations of the noninteracting LH2 complexes, part I.[54] However, it must be realized that the experiments have been performed on ensembles of clusters that vary in size and shape. Furthermore, a phospholipid bilayer is not a rigid structure and the mutual distances of the LH2 complexes are not uniform. Finally, it cannot be excluded that the reconstitution process leads to some LH2 complexes that are oriented upside down with respect to each other. These uncertainties lead to variations in the energy transfer efficiency which depends sensitively on the distance between the donor and acceptor states involved in the process.[45] In other words, the energy transfer rate as well as the size and/or the shape of the clusters are subjected to distributions. In contrast to the experimental reality, the simulations are performed on model clusters of equal size/shape comprising perfectly arranged LH2 complexes featuring identical energy transfer rates between adjacent LH2 complexes.

In order to test the influence of variations of the above-mentioned parameters on the fluorescence transients, the simulations were repeated as a function of both the size/shape of the model clusters and the magnitude of the energy transfer rate. The size of the arrays was varied from (2×2) to (14×14) hexagonally arranged LH2 complexes and the results of the simulations are shown in Figure 9A for a fluence of 26×10^{12} photons/(pulse·cm^2) and at a repetition rate of 81 MHz. These simulations clearly reveal that the amplitude of the fast decay component depends on the cluster size and increases for larger
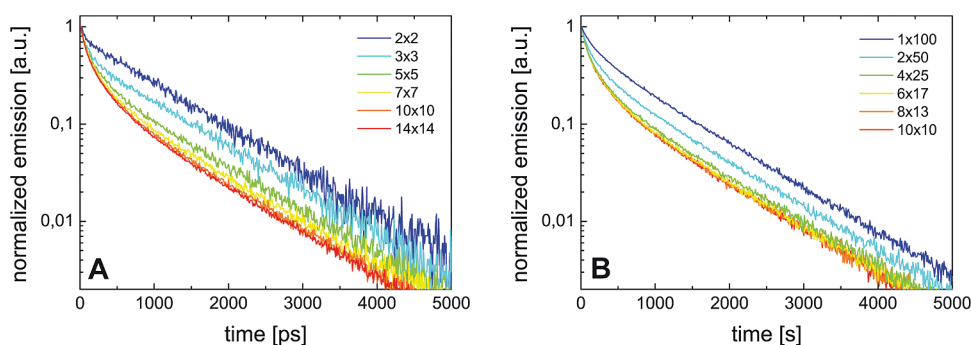
Figure 9. Simulated fluorescence decay curves for a repetition rate of 81 MHz and an excitation fluence of 26×10^{12} photons/(pulse·cm²). **(A)** As a function of LH2 cluster size: 2×2 (blue), 3×3 (cyan), 5×5 (green), 7×7 (yellow), 10×10 (orange), 14×14 (red). **B:** As a function of the shape of the LH2 cluster: 1×100 (blue), 2×50 (cyan), 4×25 (green), 6×17 (yellow), 8×13 (orange), 10×10 (red). All transients have been normalized for better comparison.
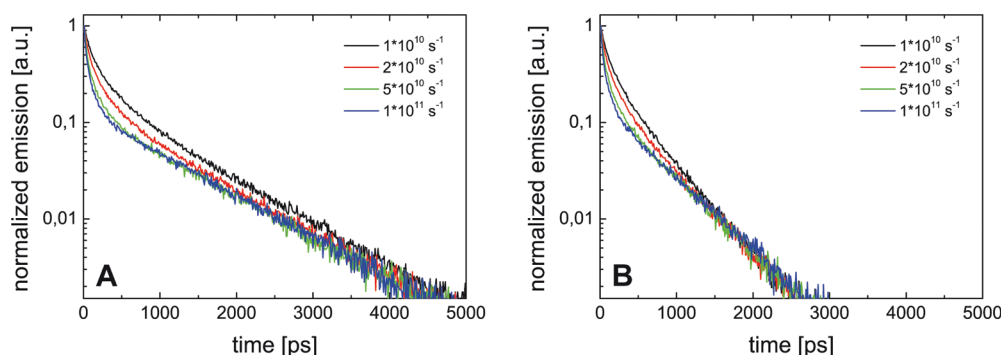

Figure 10. Simulated fluorescence decay curves within a cluster of 61 LH2 complexes for a repetition rate of 81 MHz and an excitation fluence of 26×10^{12} photons/(pulse·cm²) as a function of the energy transfer rate k_{ET}: 1×10^{10} s^{-1} (black), 2×10^{10} s^{-1} (red), 5×10^{10} s^{-1} (green) and 1×10^{11} s^{-1} (blue). **A:** For the quenching rate $k_{q,43} = 1.8 \times 10^8$ s^{-1}. **B:** For the quenching rate $k_{q,43} = 2 \times 10^9$ s^{-1}.

clusters. The larger the cluster, the more ^{1}B850* excitations are present and can be quenched by singlet−singlet annihilation. Moreover, the results shown in Figure 9A reveal that the increase of the amplitude of the fast component levels off at cluster sizes around 10×10 LH2 complexes. Apparently, for clusters larger than this, the remaining ^{1}B850* excitations cannot find each other during their lifetime. This is consistent with the conclusions about the area that can be sampled by a single ^{1}B850* excitation within a cluster of LH2 complexes. The influence of the shape of the cluster on the fluorescence transients is addressed in the simulations shown in Figure 9B. The shape of the clusters, each containing about 100 LH2 complexes, was varied between (1×100) and (10×10). The simulations reveal that the amplitude of the fast decay component is the larger, the closer the shape of the cluster resembles a quadratic arrangement of the LH2 complexes. This shows that the energy transfer efficiency depends on the dimensionality of the transfer process, which is a well-known phenomenon seen in exciton migration in molecular crystals.[46−48] There it was found that the lower the dimensionality of the energy transfer process, the lower the chance that two excitations meet on the same crystal site, which means that losses due to singlet−singlet annihilation are less probable for a (close to) one-dimensional alignment of the LH2 complexes. It is interesting to speculate whether this finding might be of relevance for the architecture of the natural photosynthetic unit.[49−51] From these model calculations, it becomes apparent, that variations in the size and/or shape of the clusters

result in a distribution of the amplitude of the fast decay component of the fluorescent transients.

The influence of the magnitude of the energy transfer rate on the fluorescence transients is shown in Figure 10. For these simulations, again clusters of 61 hexagonally arranged LH2 complexes were examined and the fluence and the repetition rate were set to 26×10^{12} photons/(pulse·cm²) and 81 MHz, respectively. Except for the energy transfer rate, which was varied between 10^{10} s^{-1} and 10^{11} s^{-1}, the input parameters for the simulations have not been changed, see Table 2. For better comparison with the results presented in Figure 8, the simulations were carried out using 1.8×10^8 s^{-1}, Figure 10A, and 2×10^9 s^{-1}, Figure 10B, for the singlet−triplet annihilation rate k_{STA}. In both panels, a lowering of the energy transfer rate results in a decrease of the time constant of the fast decay component. This is consistent with the assignment of the fast decay to the time that elapses before two ^{1}B850* excitations meet and undergo singlet−singlet annihilation. As expected, the time constant of the slow component decreases for the simulations conducted with the larger value for k_{STA}, see Figure 10A vs Figure 10B. But interestingly, within one panel, i.e. for the same numerical value of k_{STA}, the time constant of the slow decay process decreases upon decreasing the energy transfer rate. This reflects the fact that for a lower energy transfer efficiency between LH2 complexes, the relative yield of intracomplex quenching mechanisms, such as singlet−triplet annihilation or intersystem crossing, increases resulting in a growth of the relative population of

(multiple) triplet states in the cluster. What we learn from these model calculations is that the magnitude of the energy transfer rate influences not only the frequency of singlet—singlet annihilation processes, this could have been expected, but that it also indirectly affects the population of the triplet states and thereby impacts on the frequency of singlet—triplet annihilation processes. These additional simulations confirm the qualitative statements made in the context of Figure 6, that in an array of LH2s the quenching of the fluorescence is determined by a complex interplay of annihilation processes (inter- and intracomplex) that crucially influence each others efficiencies.

From the simulations presented in Figures 9 and 10, it becomes evident that averaging over the size/shape of the clusters as well as replacing the uniform energy transfer rate by a distribution of rates and averaging over this distribution will smear out the clear biexponential fluorescence transients. Although this is not a rigid proof, it is very reasonable that the discrepancies between the experimentally observed fluorescence decays and the simulated decays do reflect the fact that the experimental curves are caused by averaging, and that our model grasps the essential dynamics within the manifold of the electronically excited states of a homoarray of LH2 complexes.

CONCLUSIONS

We performed time-resolved fluorescence measurements on homoarrays of membrane-reconstituted LH2 complexes as a function of both excitation fluence and repetition rate. The experimental data are compared with results from DMC simulations that are based on a model that allows for a simplified description of an array of multichromophoric LH2 complexes. The model takes the multichromophoric character of the LH2 complexes explicitly into account by allowing for multiple singlet or triplet excitations on the same pigment—protein complex (not to be confused with higher excited singlet or triplet states on the same BChl a or Car molecule). The DMC algorithm is particularly useful for modeling experiments with pulsed excitation, where population in long-lived triplet states can be accumulated. It allows annihilation effects to be taken into account by linear rates without having to resort to power series in the populations of the involved states and the introduction of phenomenological parameters. For the arrays of LH2 complexes, the DMC simulations reproduce qualitatively the measured data and reasonable arguments can be provided that the quantitative discrepancies are caused by ensemble-averaging effects.

If no other quenching mechanisms than radiative decay were effective for a $^1B850^*$ excitation, the energy could migrate at most within an array of about 10×10 LH2 complexes. The presence of other loss mechanisms for the excitation energy will reduce this size significantly. From our data, we find that all singlet excitations within a homoarray of 10×10 LH2 complexes are quenched to a single $^1B850^*$ excitation by singlet—singlet annihilation and singlet—triplet annihilation processes. Hence an increase of the light-harvesting efficiency cannot be achieved by absorbing more photons but requires the presence of more transducers (RC-LH1) within this area. On the basis of the dynamics of energy transfer and annihilation processes within an array of LH2 complexes, we found that for our excitation conditions, one singlet excitation can migrate only over 5—10 LH2 complexes. From these numbers, it can be estimated that about 1 RC-LH1 complex per 5—10 LH2 complexes is needed to exploit

the excitation energy for further use. Any excess of LH2 complexes above this level will result in loss of efficiency. This estimate is purely based on the photophysical properties of the LH2 complexes, and it is interesting to see that the order of magnitude of this ratio is in reasonable agreement with the 1:3 ratio (RC-LH1:LH2) that was found from geometrical constraints for the chromatophore vesicle architecture of *Rb. sphaeroides*.[45]

ASSOCIATED CONTENT

ⓈSupporting Information. Typical Cryo-TEM picture for DOPC/DOPG proteoliposomes containing LH2 complexes and a movie giving the visualization of a DMC simulation showing the excited state dynamics of a model LH2 cluster containing 61 LH2 complexes. This material is available free of charge via the Internet at http://pubs.acs.org.

AUTHOR INFORMATION

Corresponding Author
*Telephone: +49 921 55 4000. Fax: +49 921 55 4002. E-Mail: juergen.koehler@uni-bayreuth.de.

Present Addresses
‡Institut für Biomedizinische Optik, Peter-Monnik-Weg 4, 23562 Lübeck, Germany.

ACKNOWLEDGMENT

REFERENCES

(1) Blankenship, R. E. *Molecular Mechanisms of Photosynthesis*: Blackwell Science: Oxford, 2002.

(2) Cogdell, R. J.; Köhler, J. *Quantum Efficiency in Complex Systems, Part I: Biomolecular systems*; Book Series: Semiconductors and Semimetals; Academic Press and University of California: Berkeley, CA, 2010; Volume 83, pp 77—94.

(3) Feher, G.; Allen, J. P.; Okamura, M. Y.; Rees, D. C. *Nature* **1989**, *339*, 111–116.

(4) Zinth, W.; Wachtveitl, J. *ChemPhysChem* **2005**, *6*, 871–880.

(5) Hu, X.; Ritz, T.; Damjanovic, A.; Autenrieth, F.; Schulten, K. *Q. Rev. Biophys.* **2002**, *35*, 1–62.

(6) Cogdell, R. J.; Gall, A.; Köhler, J. *Q. Rev. Biophys.* **2006**, *39*, 227–324.

(7) Law, C. J.; Cogdell, R. J.; Trissl, H.-W. *Photosynt. Res.* **1997**, *52*, 157–165.

(8) Westerhuis, W. H. J.; Vos, M.; van Grondelle, R.; Amesz, J.; Niederman, R. A. *Biochim. Biophys. Acta* **1998**, *1366*, 317–329.

(9) Emerson, R.; Arnold, W. *J. Gen. Physiol.* **1932**, *16*, 191–205.

(10) Green, B. R.; Parson, W. W. *Light Harvesting Antennas in Photosynthesis*; Kluwer Academic Publishers: Dordrecht, The Netherlands, 2003.

(11) Papiz, M. Z.; Prince, S. M.; Hawthornthwaite-Lawless, A. M.; McDermott, G.; Freer, A. A.; Isaacs, N. W.; Cogdell, R. J. *Trends Plant Sci.* **1996**, *1*, 198–206.

8830

dx.doi.org/10.1021/jp2023583 |*J. Phys. Chem. B* 2011, 115, 8821–8831

(12) Cogdell, R. J.; Fyfe, P. K.; Barrett, S. J.; Prince, S. M.; Freer, A. A.; Isaacs, N. W.; McGlynn, P.; Hunter, C. N. *Photosynth. Res.* **1996**, *48*, 55–63.

(13) Monger, T. G.; Parson, W. W. *Biochim. Biophys. Acta* **1977**, *460*, 393–407.

(14) McDermott, G.; Prince, S. M.; Freer, A. A.; Hawthornthwaite-Lawless, A. M.; Papiz, M. Z.; Cogdell, R. J.; Isaacs, N. W. *Nature* **1995**, *374*, 517–521.

(15) McLuskey, K.; Prince, S. M.; Cogdell, R. J.; Isaacs, N. W. *Biochemistry* **2001**, *40*, 8783–8789.

(16) Koepke, J.; Hu, X.; Muenke, C.; Schulten, K.; Michel, H. *Structure* **1996**, *4*, 581–597.

(17) Roszak, A. W.; Howard, T. D.; Southall, J.; Gardiner, A. T.; Law, C. J.; Isaacs, N. W.; Cogdell, R. J. *Science* **2003**, *302*, 1969–1971.

(18) Qian, P.; Neil Hunter, C.; Bullough, P. A. *J. Mol. Biol.* **2005**, *349*, 948–960.

(19) Karrasch, S.; Bullough, P. A.; Ghosh, R. *EMBO J.* **1995**, *14*, 631–638.

(20) Scheuring, S.; Rigaud, J. L.; Sturgis, J. N. *EMBO J.* **2004**, *23*, 4127–4133.

(21) Fassioli, F.; Olaya-Castro, A.; Scheuring, S.; Sturgis, J. N.; Johnson, N. F. *Biophys. J.* **2009**, *97*, 2464–2473.

(22) Breton, J.; Geacintov, N. E. *Biochim. Biophys. Acta* **1980**, *594*, 1–32.

(23) den Hollander, W. T. F.; Bakker, J. G. C.; van Grondelle, R. *Biochim. Biophys. Acta* **1983**, *725*, 492–507.

(24) Bakker, J. G. C.; van Grondelle, R.; den Hollander, W. T. F. *Biochim. Biophys. Acta* **1983**, *725*, 508–518.

(25) Campillo, A. J.; Hyer, R. C.; Monger, T. G.; Parson, W. W.; Shapiro, S. L. *Proc. Natl. Acad. Sci. U.S.A.* **1977**, *74*, 1997–2001.

(26) Paillotin, G.; Swenberg, C. E.; Breton, J.; Geacintov, N. E. *Biophys. J.* **1979**, *25*, 513–533.

(27) Nagarajan, V.; Parson, W. W. *Biochemistry* **1997**, *36*, 2300.

(28) Gardiner, A. T.; Cogdell, R. J.; Takaichi, S. *Photosynth. Res.* **1993**, *38*, 159–167.

(29) Cogdell, R. J.; Durant, I.; Valentine, J.; Lindsay, J. G.; Schmidt, K. *Biochim. Biophys. Acta* **1983**, *722*, 427–435.

(30) Richter, M. F.; Baier, J.; Cogdell, R. J.; Köhler, J.; Oellerich, S. *Biophys. J.* **2007**, *93*, 183–191.

(31) Stamouli, A.; Kafi, S.; Klein, D. C. G.; Oosterkamp, T. H.; Frenken, J. W. M.; Cogdell, R. J.; Aartsma, T. J. *Biophys. J.* **2003**, *84*, 2483–2491.

(32) Goncalves, R. P.; Busselez, J.; Levy, D.; Seguin, J.; Scheuring, S. *J. Struct. Biol.* **2005**, *149*, 79–86.

(33) Walz, T.; Jamieson, S. J.; Bowers, C. M.; Bullough, P. A.; Hunter, C. N. *J. Mol. Biol.* **1998**, *282*, 833–845.

(34) Pflock, T.; Dezi, M.; Venturoli, G.; Cogdell, R.; Köhler, J.; Oellerich, S. *Photosynth. Res.* **2008**, *95*, 291–298.

(35) Hofkens, J.; Cotlet, M.; Vosch, T.; Tinnefeld, P.; Weston, K. D.; Ego, C.; Grimsdale, A.; Müllen, K.; Beljonne, D.; Bredas, J. L.; Jordens, S.; Schweitzer, G.; Sauer, M.; de Schryver, F. *Proc. Natl. Acad. Sci. U.S.A.* **2003**, *100*, 13146–13151.

(36) Cogdell, R. J.; Frank, H. A. *Biochim. Biophys. Acta* **1987**, *895*, 63–79.

(37) Becker, T.; Ullmann, R. T.; Ullmann, G. M. *J. Phys. Chem. B* **2007**, *111*, 2957–2968.

(38) Till, M. S.; Essigke, T.; Becker, T.; Ullmann, G. M. *J. Phys. Chem. B* **2008**, *112*, 13401–13410.

(39) Brüggemann, B.; Herek, J. L.; Sundström, V.; Pullerits, T.; May, V. *J. Phys. Chem. B* **2001**, *105*, 11391–11394.

(40) Trinkunas, G.; Herek, J. L.; Polívka, T.; Sundström, V.; Pullerits, T. *Phys. Rev. Lett.* **2001**, *86*, 4167.

(41) Schubert, A.; Stenstam, A.; Beenken, W. J. D.; Herek, J. L.; Cogdell, R.; Pullerits, T.; Sundström, V. *Biophys. J.* **2004**, *86*, 2363–2373.

(42) Strümpfer, J.; Schulten, K. *J. Chem. Phys.* **2009**, *131*, 225101–9.

(43) Strümpfer, J.; Schulten, K. *J. Chem. Phys.* **2011**, *134*, 1–9.

(44) Agarwal, R.; Rizvi, A. H.; Prall, B. S.; Olsen, J. D.; Hunter, C. N.; Fleming, G. R. *J. Phys. Chem. A* **2002**, *106*, 7573–7578.

(45) Şener, M.; Strümpfer, J.; Timney, J. A.; Freiberg, A.; Hunter, C. N.; Schulten, K. *Biophys. J.* **2010**, *99*, 67–75.

(46) Kenkre, V. M.; Reineker, P. M. *Exciton Dynamics in Molecular Crystals and Aggregates*; Springer: Berlin, 1982.

(47) Kenkre, V. M.; Schmid, D. *Chem. Phys. Lett.* **1983**, *94*, 603–608.

(48) Köhler, J.; Schmid, D. *J. Phys.: Condens. Matter* **1996**, *8*, 115–141.

(49) Bahatyrova, S.; Frese, R. N.; Siebert, C. A.; Olsen, J. D.; van der Werf, K. O.; van Grondelle, R.; Niederman, R. A.; Bullough, P. A.; Otto, C.; Hunter, C. N. *Nature* **2004**, *430*, 1058–1062.

(50) Frese, N. R.; Siebert, A. C.; Niederman, R. A.; Hunter, C. N.; Otto, C.; van Grondelle, R. *Proc. Natl. Acad. Sci. U.S.A.* **2004**, *101*, 17994–17999.

(51) Sener, M. K.; Olsen, J. D.; Hunter, C. N.; Schulten, K. *Proc. Natl. Acad. Sci. U.S.A.* **2007**, *104*, 15723–15728.

(52) Monger, T. G.; Cogdell, R. J.; Parson, W. W. *Biochim. Biophys. Acta* **1976**, *449*, 136–153.

(53) Bittl, R.; Schlodder, E.; Geisenheimer, I.; Lubitz, W.; Cogdell, R. J. *J. Phys. Chem. B* **2001**, *105*, 5525–5535.

(54) Pflock, T.; Oellerich, S.; Southall, J.; Cogdell, R. J.; Ullmann, G. M.; Köhler, J. *J. Phys. Chem. B* **2011** 10.1021/jp202353c.